Supporting Information

Selective Proton-Coupled Electron Transfer Regulated by Potential of Zero Charge for CO_2 Electroreduction on Tailored Cobalt Phthalocyanine

Yuefei Zhang[1], Xinyu Wang[1], Haoran Yue[1], Yang Zhang[1], Lin-Wang Wang[2*], Guoping Gao[1*]

[1] MOE Key Laboratory for Non-equilibrium Synthesis and Modulation of Condensed Matter, Shaanxi Province Key Laboratory of Advanced Functional Materials and Mesoscopic Physics, School of Physics, Xi'an Jiaotong University, Xi'an, Shaanxi 710049, China

[2] State key laboratory of superlattices and microstructures, Institute of Semiconductors, Chinese Academy of Sciences, Beijing 100083, China

Email: lwwang@semi.ac.cn; guopinggao@xjtu.edu.cn

Table S1: CoPc-based molecular catalysts for CO_2RR, including their substrates, terminal groups, electrolytes, applied potentials (E), product selectivities, current densities (J_0), and corresponding references.

substrate	CoPc	Electrolyte	E	Selectivity (%)	J_0	Reference
Carbon	CoPc1	0.5 M $NaHCO_3$	-0.68	92 for CO	13.1 (mA cm^{-2})	1
Carbon	CoPc2	0.5 M KCl	-0.97	92 for CO	16.3 (mA cm^{-2})	1
Carbon	CoPc2	0.5 M $NaHCO_3$	-0.68	93 for CO	18.1 (mA cm^{-2})	1
Carbon	CoPc2	1 M KOH	-0.31	93 for CO	22.2 (mA cm^{-2})	1
Carbon	CoPc2	1 M KOH	-0.65	94 for CO	70.5 (mA cm^{-2})	1
Carbon	CoPc2	1 M KOH	-0.72	96 for CO	111.6 (mA cm^{-2})	1
Carbon	CoPc2	1 M KOH	-0.92	94 for CO	165 (mA cm^{-2})	1
CNT	CoPc	0.1 M $KHCO_3$	-0.63	92 for CO	~10 (mA cm^{-2})	2
CNT	CoPc-CN	0.1 M $KHCO_3$	-0.63	98 for CO	~15 (mA cm^{-2})	2
CNT	CoPc-CN	0.5 M $NaHCO_3$	-0.46	88 for CO	~5.6 (mA cm^{-2})	2
CNT	CoPcpc	0.5 M $NaHCO_3$	-0.61	ca. 90	18 (mA cm^{-2})	3
MWCNTs	CoPc(qpy)	0.5 M $NaHCO_3$	-0.55	99 for CO	19.9 (mA cm^{-2})	4
carbon cloth electrode	Perfluorinated CoPc	0.5 M $KHCO_3$	-0.80	93 for CO	4.4 (mA cm^{-2})	5
/	COF-367-Co	0.5M $KHCO_3$	-0.67	91 for CO	3.3 (mA cm^{-2})	6
CNT-MD	CoPc	0.5M $KHCO_3$	−0.90	97 for CO	−38.72 (mA cm^{-2})	7
CNT-AG	CoPc	0.5M $KHCO_3$	−0.7	90 for CO	−36.72 (mA cm^{-2})	7
carbon black	MOF-1992	$KHCO_3$	−0.52	80 for CO	−16.5 (mA cm^{-2})	8
CNT-ODA	CoPc	0.5 M $KHCO_3$	-1.00	97.7 for CO	154.8 (mA cm^{-2})	9

carbon powder	CoPc	1 M KOH	Ecellof 2.5	> 95% for CO	150 (mA cm^{-2})	[10]
Carbon	CoPc	0.05 M citrate buffer	−1.15Vvs.SCE	87 for CO	0.98 (mA cm^{-2})	[11]
CNT	CoPc	0.5 M $KHCO_3$	− 1.3 V vs. SCE	70 for CO	50 ~ 70 (mA cm^{-2})	[12]
CNT	CoPc	0.05 M K_2CO_3	− 0.7 V vs. SCE	86 for CO	1.3 (mA cm^{-2})	[13]
CNT	CoPc	0.1 M $KHCO_3$	-0.61	90 for CO	− 1.0 (mA cm^{-2})	[14]
rGO	CoPc	0.75 M $NaHCO_3$	-0.60	95.5 for CO	7.5 (mA cm^{-2})	[15]
acetylene black	CoPc	0.1 M $KHCO_3$	-0.70	99.8 for CO	11.6 (mA cm^{-2})	[16]
/	N−C−CoPc NR	0.1 M $KHCO_3$	-0.70	85.3 for CO	6 (mA cm^{-2})	[17]
NRGO	N-CoMe2Pc	1 M KOH	-0.60	94.1 for CO	56.4 (mA cm^{-2})	[18]
OxC	CoPc	0.1 M $NaHCO_3$	-0.73	96 for CO	2.4 (mA cm^{-2})	[19]
carbon paper	CoPc-1	0.5 M $KHCO_3$	–0.54	94 for CO	2.2 (mA cm^{-2})	[20]
CFP	CoTNPc	0.5 M $KHCO_3$	-0.88	94 for CO	12.6 (mA cm^{-2})	[21]
CFP	CoOCPc	0.5 M $KHCO_3$	-0.78	91 for CO	6.8 (mA cm^{-2})	[21]
HCS-x(x =1-9)	CoPc	0.5 M $KHCO_3$	-0.82	91 for CO	-14 (mA cm^{-2})	[22]
Carbon cloth	CoPc	0.5 M $KHCO_3$	−1.08	99% for CO	46.1 (mA cm^{-2})	[23]
CNTs	CoPc-4OCH_3	1 M KOH	−0.6 to −0.9	91% for CO	48.7 (mA cm^{-2})	[24]
CNTs	CoPc-4NO_2	1 M KOH	−0.8 to −0.9 V	90% for CO	34.3 (mA cm^{-2})	[24]
CNTs	CoPc	1 M KOH	−0.8 to −0.9 V	89% for CO	10.8 (mA cm^{-2})	[24]
PNCA	CoPPc	1 M KOH	-1.8 V	~100% for CO	210 (mA cm^{-2})	[25]
Carbon	M-CoPc-400	0.5 M KOH	-0.7 V	19% for MeOH	26 (mA cm^{-2})	[26]
Carbon	B-CoPc-400	0.5 M KOH	-0.8 V	50% for MeOH	35 (mA cm^{-2})	[26]
/	PEH-COF	0.1 M NaOH	-1.6 V	38.5% for MeOH	100.9 (mAcm^{-2})	[27]
CNTs	CoPc-NH_2	0.3 M $KHCO_3$	-0.9 V	32% for MeOH	129 (mA cm^{-2})	[28]
CNTs	CoPc	0.1 M $KHCO_3$	-0.96 V	41% for MeOH	7.3 (mA cm^{-2})	[29]
MWCNTs	CoTAPc	0.5 M $KHCO_3$	-1.37 V_{RHE}	62% for MeOH	132 (mA cm^{-2})	[30]
MWCNT	CoPc	0.5 M $KHCO_3$	–0.9 V	12% for MeOH	12 (mA cm^{-2})	[31]
CNTs	CoPc	0.1 M $KHCO_3$	-0.94 V	44% for MeOH	10.6 (mA cm^{-2})	[32]
CNTs	CoPc-NH_2	0.1 M $KHCO_3$	-1.00 V	41% for MeOH	10.2 (mA cm^{-2})	[32]
CNTs	CoPc-NH_2	0.1 M KOH	-0.95 V	45% for MeOH	12 (mA cm^{-2})	[33]
CNTs	NiPc-OCH_3/CoPc-NH_2	0.1 M $KHCO_3$	-0.98 V	50% for MeOH	150 (mA cm^{-2})	[34]
CNTs	CoPc-NH_2	0.1 M $KHCO_3$	-0.98 V	84% for MeOH (CO to MeOH)	20 (mA cm^{-2})	[35]

Note 1: Calcuation of the formation energy and link to the charge transfer in GC-DFT

To highlight the fixed-potential method (FPM) in CO_2RR, we first compare the CO_2 adsorption and the first hydrogenation step (CO_2 to CO) between the computation hydrogen electrode (CHE) and FPM. In CHE, the adsorption of CO_2 and the first

hydrogenation step can be expressed as:

$$CO_2 + * \rightarrow *CO_2 \quad (1)$$

$$*CO_2 + H^+ + e^- \rightarrow *COOH \quad (2)$$

$$*COOH + H^+ + e^- \rightarrow *CO + H_2O \quad (3)$$

$$*CO \rightarrow * + CO\ (g) \quad (4)$$

when considering the ideal standard hydrogen electrode (SHE) corresponding to the absolute potential (Uabs), the relationship between U_{abs} and the electrochemical potential (V vs. SHE) can be expressed as $U_{SHE} = -(U_{abs} + 4.44)$. Subsequently, the Gibbs free energy of this two steps can be calculated as follow:

$$\Delta G_{*CO_2} = G_{*CO_2} - G_{CO_2} - G_* \quad (5)$$

$$\Delta G_{*COOH} = G_{*COOH} - \left(\frac{1}{2}G_{H_2} + 4.44e\right) - G_{*CO_2} - kT\ln 10 \times pH - eU_{abs}$$

$$= G_{*COOH} - \frac{1}{2}G_{H_2} - G_{*CO_2} - kT\ln 10 \times pH + eU_{SHE} \quad (6)$$

$$\Delta G_{*CO} = G_{*CO} + G_{H_2O} - \left(\frac{1}{2}G_{H_2} + 4.44e\right) - G_{*COOH} - kT\ln 10 \times pH - eU_{abs}$$

$$= G_{*CO} + G_{H_2O} - \frac{1}{2}G_{H_2} - G_{*COOH} - kT\ln 10 \times pH + eU_{SHE} \quad (7)$$

in which the *, k, T stand for the electrode substrate, Boltzmann constant, and the temperature. When considering the applied potential effect, the two steps under the FPM could be ascribed as:

$$CO_2 + *^{q_1} \rightarrow *CO_2^{q_2} + (q_2 - q_1)e^- \quad (8)$$

$$*CO_2^{q_2} + \left(H^+ + e^-\right) \rightarrow *COOH^{q_3} + \left(q_3 - q_2\right)e^-$$

$$= *CO_2^{q_2} + H^+ \rightarrow *COOH^{q_3} + (q_3 - q_2 - 1)e^- \quad (9)$$

$$*COOH^{q_3} + (H^+ + e^-) \rightarrow *CO^{q_4} + H_2O + (q_4 - q_3)e^-$$

$$= *COOH^{q_3} + H^+ \rightarrow *CO^{q_4} + H_2O + (q_4 - q_3 - 1)e^- \quad (10)$$

Where q_1, q_2, q_3 are the charge state of the bare electrode, the electrode with CO_2 adsorbed, and the electrode with COOH adsrobed under the applied potential U_{abs}, respectively. The corresponding reaction energy of this two steps can be calculated by:

$$\Delta G_{FPM}^{1} = G_{*CO_2}^{q_2} - G_{*}^{q_1} - G_{CO_2} + (q_2 - q_1)eU_{abs}$$

$$= \left(G_{*CO_2}^{q_2} + q_2 eU_{abs}\right) - \left(G_{*}^{q_1} + q_1 eU_{abs}\right) - G_{CO_2} \quad (11)$$

$$\Delta G_{FPM}^{2} = G_{*COOH}^{q_3} - G_{*CO_2}^{q_2} - \frac{1}{2}G_{H_2} - 4.44e - k\mathrm{Tln}10 \times \mathrm{pH} + (q_3 - q$$

$$= \left(G_{*COOH}^{q_3} + q_3 eU_{abs}\right) - \left(G_{*CO_2}^{q_2} + q_2 eU_{abs}\right) - k\mathrm{Tln}10 \times \mathrm{pH} - e(U_{abs} + 4.44) \quad (12)$$

$$\Delta G_{FPM}^{3} = G_{*CO}^{q_4} + G_{H_2O} - G_{*COOH}^{q_3} - \frac{1}{2}G_{H_2} - 4.44e - k\mathrm{Tln}10 \times \mathrm{pH} + (q_4 - q_3 - eU_{abs}$$

$$= \left(G_{*CO}^{q_4} + q_4 eU_{abs}\right) + G_{H_2O} - \left(G_{*COOH}^{q_3} + q_3 eU_{abs}\right) - k\mathrm{Tln}10 \times \mathrm{pH} - e(U_{a}$$

(9)

here, we can define the grand energy $E_{grand} = E^q + qeU_{abs}$ and grand free energy $G_{grand} = G_q + qeU_{abs}$, and the Gibbs free energy can be described as:

$$\Delta G_{FPM}^{1} = G_{*CO_2,grand} - G_{*,grand} - G_{CO_2} \quad (13)$$

$$\Delta G_{FPM}^{2} = G_{*COOH,grand} - G_{*CO_2,grand} - \frac{1}{2}H_2 - k\mathrm{Tln}10 \times \mathrm{pH} + eU_{SHE} \quad (14)$$

$$\Delta G_{FPM}^{3} = G_{*CO,grand} + G_{H_2O} - G_{*COOH,grand} - \frac{1}{2}H_2 - k\mathrm{Tln}10 \times \mathrm{pH} + eU_{SHE} \quad (15)$$

therefore, for the CO_2RR progress, the Gibbs free energy can be obtained from equal

(9) and (10) for the electron transfer (ET) and proton coupling electron transfer (PCET) process.

Meanwhile, in this work, we assume the applied potential is fixed, and the PZC is the controlled variable. According to the definition of the potential-dependent free energy, the applied potential could form a quadratic function with the U_{SHE}:

$$G_{\alpha,grand}(U_{abs}) = -\frac{1}{2}C(U_{abs} - PZC_{\alpha})^2 + G_{\alpha}^{PZC} \tag{16}$$

where C is the capacitance, which can be approximately equal due to constant active site and coordination environment, PZC_{α} is the PZC of the CoPc (PZC_{*}) or the intermediate-adsorbed CoPc systems, and G_{α}^{PZC} is the free energy of systems at PZC. Under ideal condition, suppose that the PZC_{*} changes while the U_{SHE} keep constant for an identified materials, the $G_{\alpha,grand}(U_{SHE})$ and the PZC still exhibit a quadratic function. In fact, the PZC-dependent free energy can not show similar quadratic function with the PZC due to the structure variation induced energy changes. In contract, the PZC-dependent free energy changes of intermediate (such as CO_2) may show quadratic function as described by:

$$\Delta G_{*CO_2,grand}(U_{SHE}) = -\frac{1}{2}C\left[(U_{SHE} - PZC_{*CO_2})^2 - (U_{SHE} - PZC_{*})^2\right] + \Delta G_{*CO_2}^{PZC} - N_{*CO_2} \times e U_{SHE}$$

$$= \Delta G_{*CO_2}^{PZC} - \frac{1}{2}C\left[(PZC_{*CO_2})^2 - (PZC_{*})^2\right] - \left[eN_{*CO_2} - C(PZC_{*CO_2} - PZC_{*})\right]U_{SHE} \tag{17}$$

among them, $\Delta G_{*CO_2}^{PZC}$, PZC_{*CO_2}, N_{*CO_2} are the free energy changes of adsorbed CO_2 at PZC, the PZC of the CO_2 adsorbed CoPc system, and the charge transfer value of CO_2 at PZC. Notably, due to the constant C, U_{SHE}, as well as the $\Delta G_{*CO_2}^{PZC}$, eN_{*CO_2} at PZC, the changes of the free energy mainly impacted by the PZC_{*CO_2} and PZC_{*},

which make $-\frac{1}{2}C\left[\left(PZC_{*CO_2}\right)^2 - \left(PZC_{*}\right)^2\right]$ and $\left[eN_{*CO_2} - C\left(PZC_{*CO_2} - PZC_{*}\right)\right]U_{SHE}$ become the determined term for controlling the quadratic function or linear function under the PZC variable. Meanwhile, the ΔPZC ($PZC_{*\alpha} - PZC_{*}$, $\frac{N_{*CO_2} - C\left(PZC_{*CO_2} - PZC_{*}\right)}{e}$ is the revised charge transfer values) is controlled by the charge transfer between the active site and the adsorbed intermediates, making the charge dynamically transfer and accumulation become the key to the catalytic performance, thereby controlling the catalytic activities.

Note2: Calculation of the Microkinetic models

The microkinetic model for the CO_2RR to CO was constructed based on recent mechanistic studies. It incorporates the **elementary reaction steps** from CO_2 adsorption to CO desorption, as outlined below:

$$CO_2 + * \rightarrow *CO_2 \quad (20)$$

$$*CO_2 + H^+ + e^- \rightarrow *COOH \quad (21)$$

$$*COOH + H^+ + e^- \rightarrow *CO + H_2O \quad (22)$$

$$*CO \rightarrow CO \quad (23)$$

Where the rate equation of each intermediate could expressed by:

$$\frac{\partial\theta_*}{\partial t} = k_4\theta_{*CO} - k_{-4}p_{CO}\theta_* - k_1\chi_{CO2}\theta_* + k_{-1}\theta_{*CO2} \quad (24)$$

$$\frac{\partial\theta_{*CO2}}{\partial t} = k_1\chi_{CO2} - k_{-1}\theta_{*CO2} - k_2\theta_{*CO2} + k_{-2}\theta_{*COOH} \quad (25)$$

$$\frac{\partial\theta_{*COOH}}{\partial t} = -k_{-2}\theta_{*COOH} + k_2\theta_{*CO2} + k_{-3}\theta_{*CO} - k_3\theta_{*COOH} \quad (26)$$

$$\frac{\partial\theta_{*CO}}{\partial t} = k_3\theta_{*COOH} + k_{-3}\theta_{*CO} - k_4\theta_{*CO} + k_{-4}p_{CO}\theta_* \quad (27)$$

In this model, the θ epresents the coverage of intermediate species, χ_{CO2} denotes the equilibrium

concentration of dissolved CO_2 in the electrolyte, taken as 5.79×10-4 mol/cm^3, p_{CO} is the partial pressure of gaseous CO, fixed at 1 bar, The rate constant k is calculated using transition state theory:

$$k_i = A_i \exp\left(-\frac{\Delta G^{\ddagger}(U)}{K_B T}\right) \tag{28}$$

Where A_i is the effective prefactor, which is set to be 10 ×108 and 6.21 ×1012, KB is the Boltzmann constant,T is temperature, R is the gas constant, and $\Delta G^{\ddagger}$ is the kinetic barriers, which is set to be 0.3.

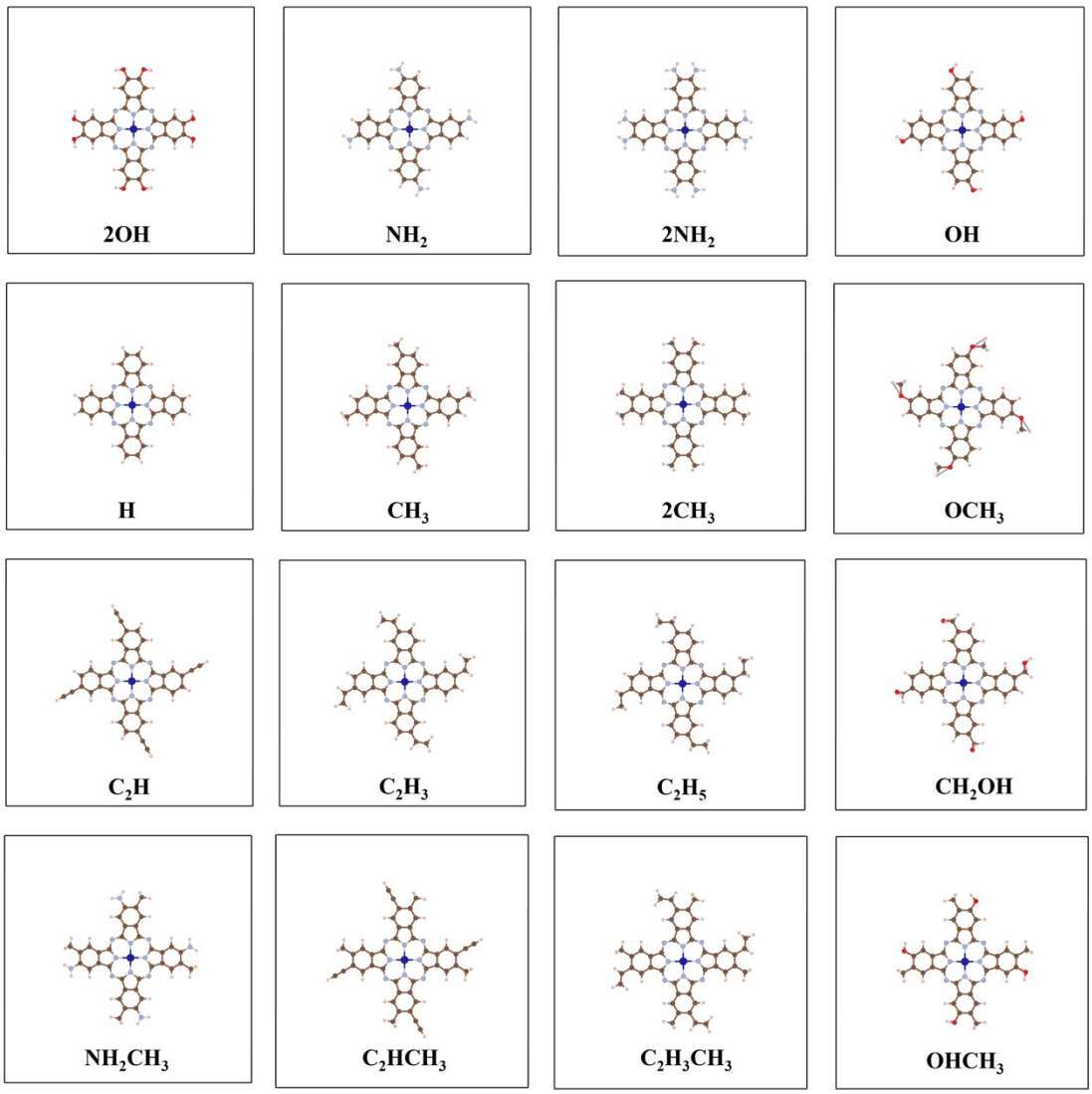

Figure S1: Geometric structure of the termination group modified CoPc.

Table S2: Bond length between the active Co site and the coordinated N atoms for varous termination groups modified CoPc.

CoPc	Co-N1	Co-N2	Co-N3	Co-N4
2OH	1.89638	1.89531	1.89439	1.89534
NH_2	1.89725	1.89566	1.89438	1.89698
$2NH_2$	1.89615	1.89473	1.89333	1.89628
NH_2CH_3	1.89723	1.89637	1.89564	1.89621
OH	1.89769	1.89673	1.89511	1.89727
$OHCH_3$	1.89656	1.89657	1.89535	1.89507
OCH_3	1.89535	1.89627	1.89673	1.89628
CH	1.89774	1.89838	1.89544	1.89741
CH_2OH	1.89626	1.89788	1.89820	1.89827
CH_3	1.89832	1.89677	1.89827	1.89755
$2CH_3$	1.89686	1.89520	1.89514	1.89768
C_2H	1.89777	1.89702	1.89647	1.89777
C_2H_3	1.89717	1.89651	1.89524	1.89752
C_2H_5	1.89724	1.89631	1.89651	1.89750
C_2HCH_3	1.89716	1.89696	1.89609	1.89680
$C_2H_3CH_3$	1.89550	1.89826	1.89365	1.89772

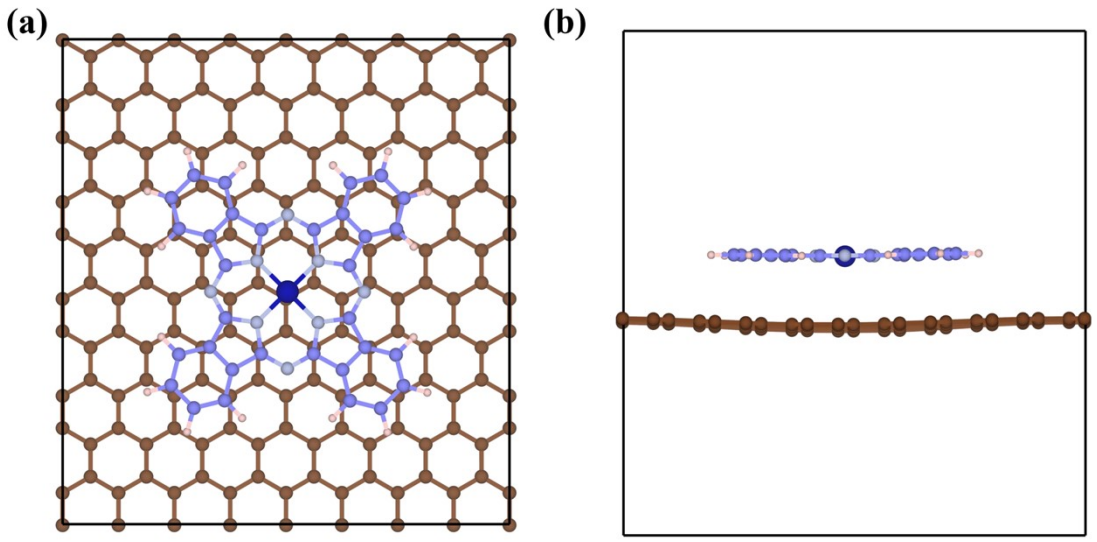

Figure S2: top and side view of the graphene/CoPc heterostructure.

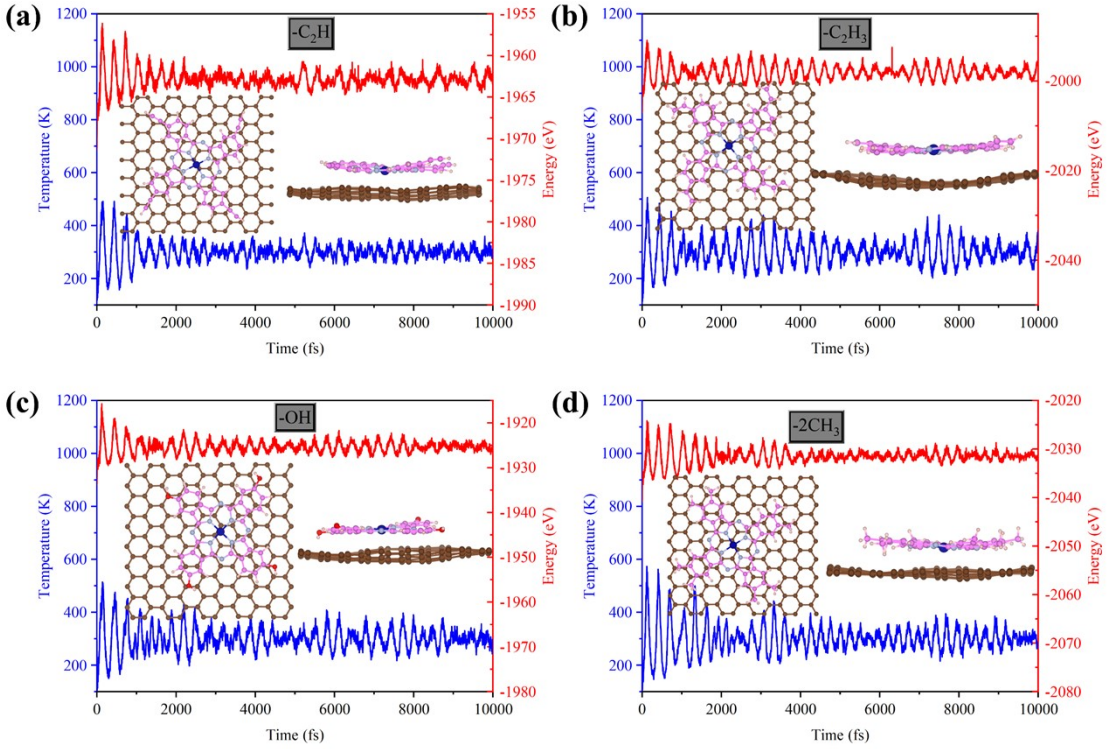

Figure S3: ab initial molecular dynamics simulation for the selected four systems: $-C_2H$, $-C_2H_3$, -OH, and $-2CH_3$ at temperature of 300K lasting for 10 ps.

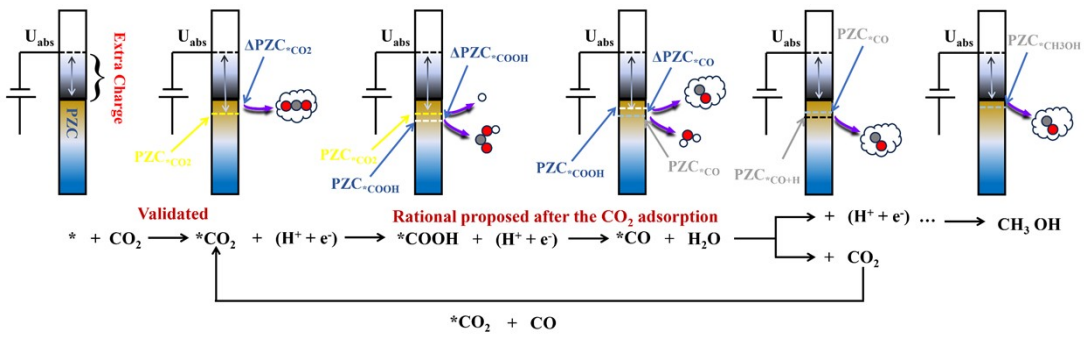

Figure S4: graphic diagram of PZC variation for the adsrobed intermediate related to the charge transfer in the adsorbed intermediates.

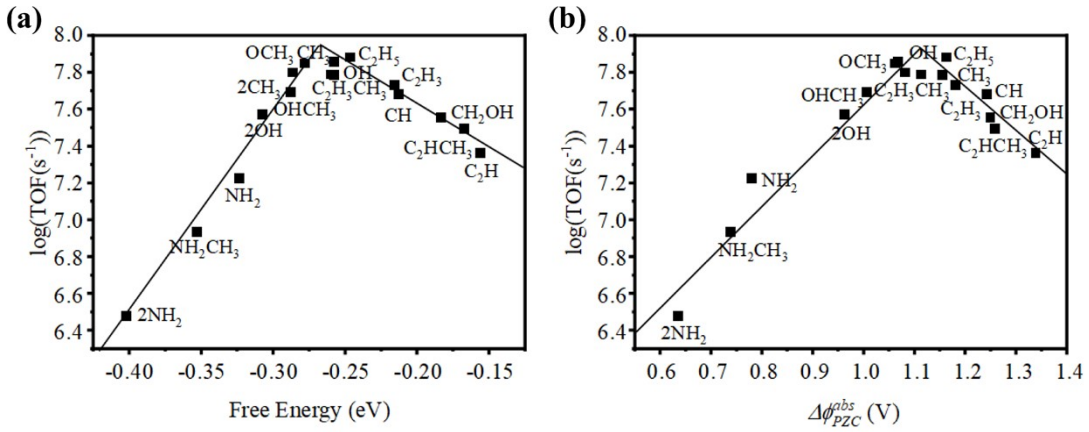

Figure S5: formation energy of COOH (a) and $\Delta\phi_{PZC}^{abs}$, (b) as function of the TOF of CO_2 to CO for the 16 kinds of graphene/CoPc catalysts under U_{abs} = -3.64 V.

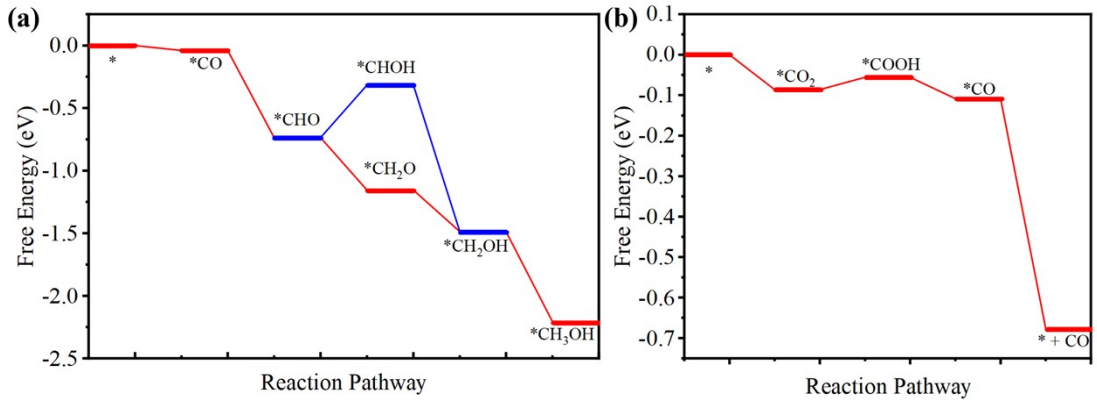

Figure S6: Gibbs free energy of the (a) CO to CH_3OH and (b) CO_2 to CO for CoPc/graphene under the working condition (U_{abs} = -3.74 V).

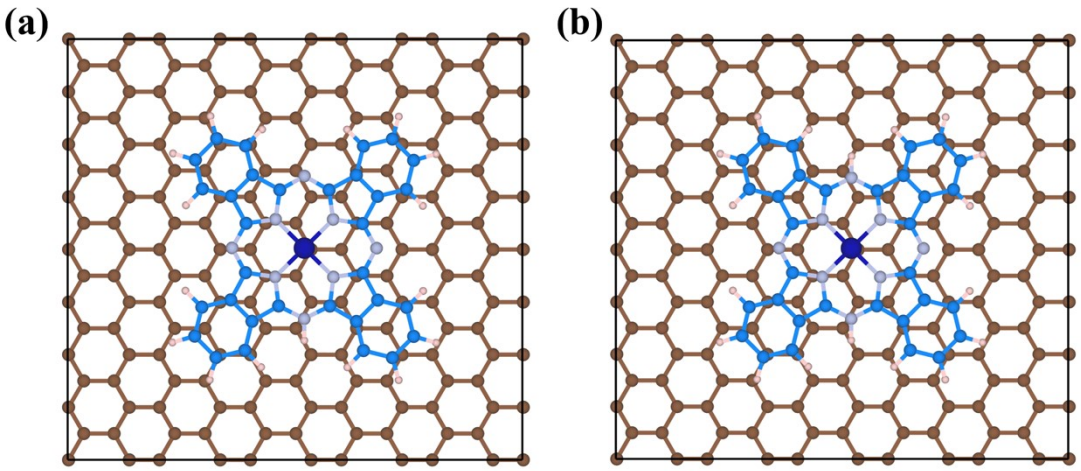

Figure S7: Geometric stuctures of the first and second prontated bridge N atom on CoPc/graphene.

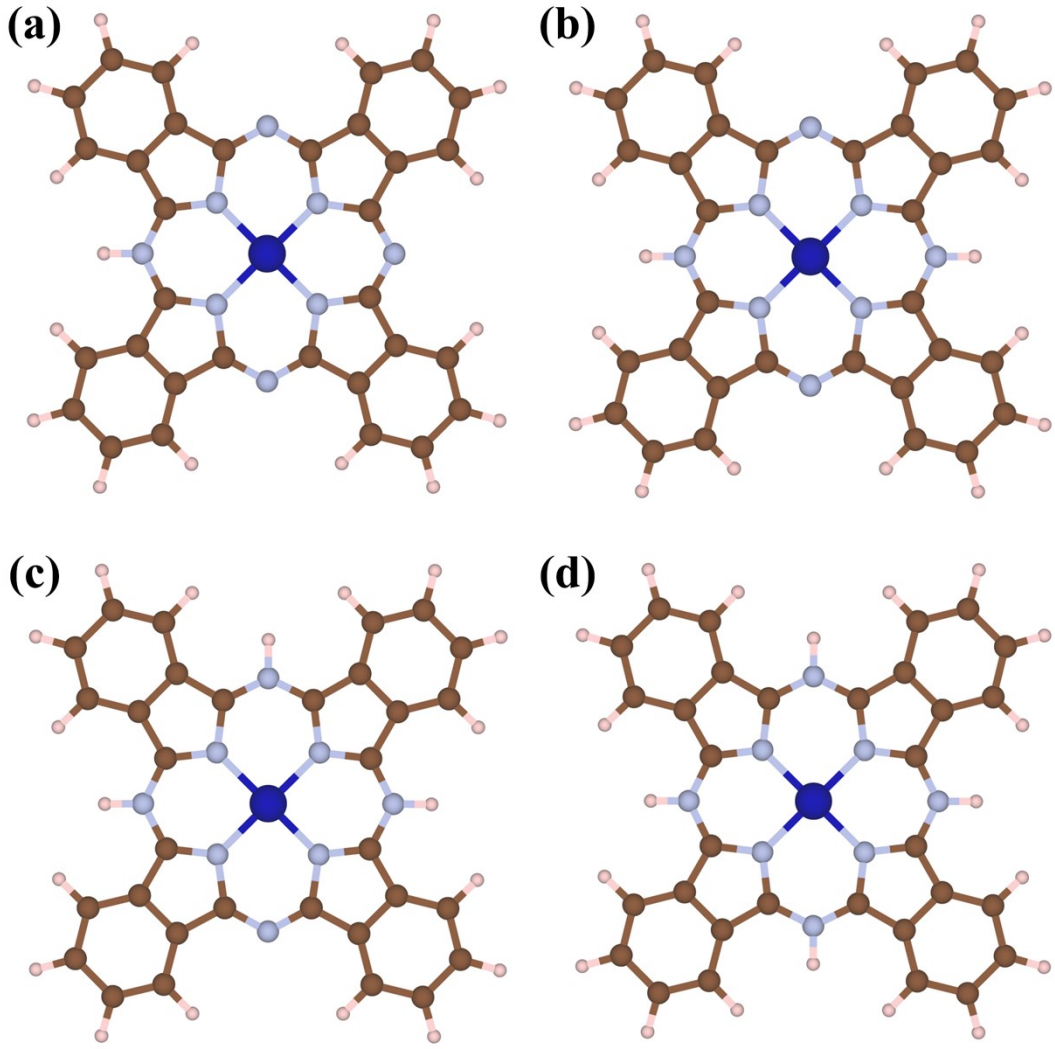

Figure S8: (a)-(d) Geometric stuctures of the prontated bridge N atom on CoPc.

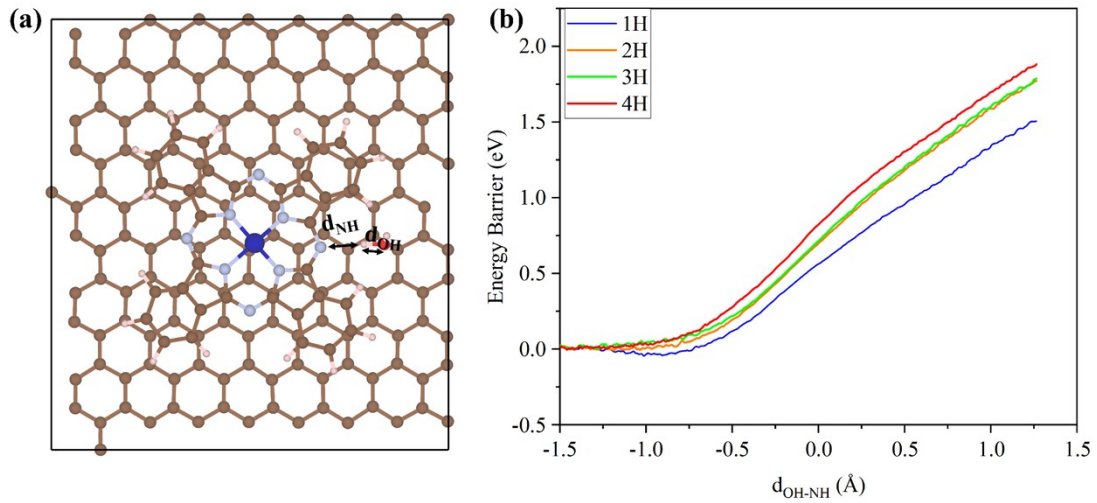

Figure S9: (a) geometric structure of the protonated site and the protonate reaction pathway and (b) the corresponding energy barriers for the first, second, third, and fourth protonation process.

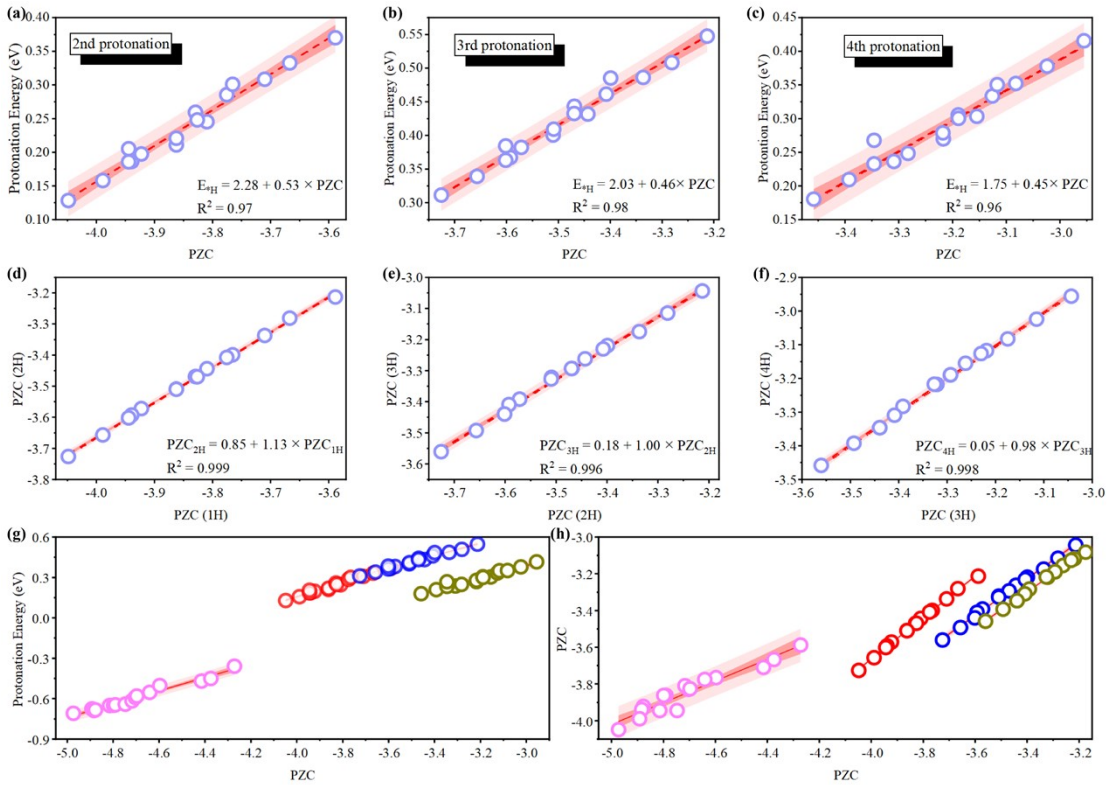

Figure S10: The protonation energy of the second (a), third (b), and fourth (c) as function of the PZC of the second, third, and fourth protonated PZC; (d)-(f) the PZC evolution with the protonated PZC for the second to fourth protonation process; (g) protonation energy as function of the PZC across the pristine to full protonation process; (h) PZC self-evolution across the whole protonation process.

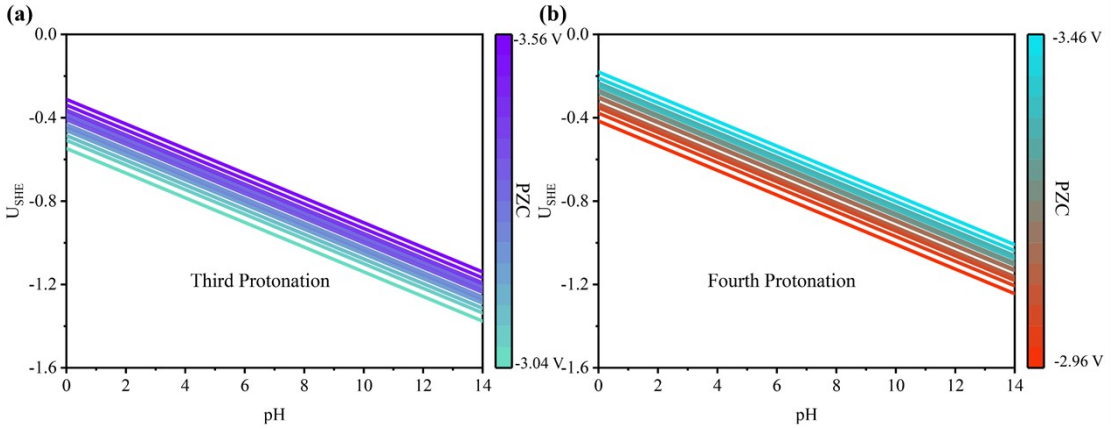

Figure S11: Pourbaix diagram for selected CoPc systems intergreted from the relation between PZC and the protonation energy for the third (a) and fourth (b) protonation process.

Figure S12: Geometric structure of the first (a) and secondary (b) protonation on CoPc/graphene systems under U_{abs} = -3.64 V (0.8 V *vs.* SHE).

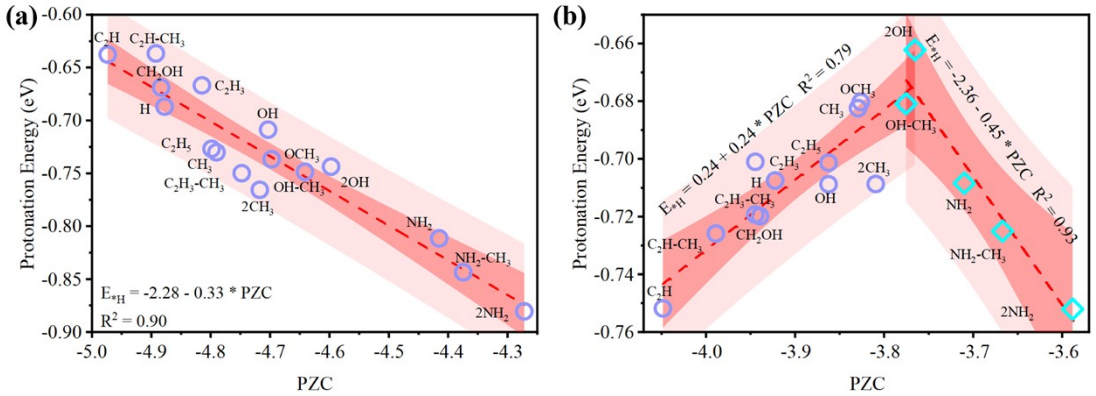

Figure S13: PZC as function of protonation energy for the first and secondary prontaontion on CoPc/graphene systems under U_{abs} = -3.64 V (0.8 V *vs.* SHE).

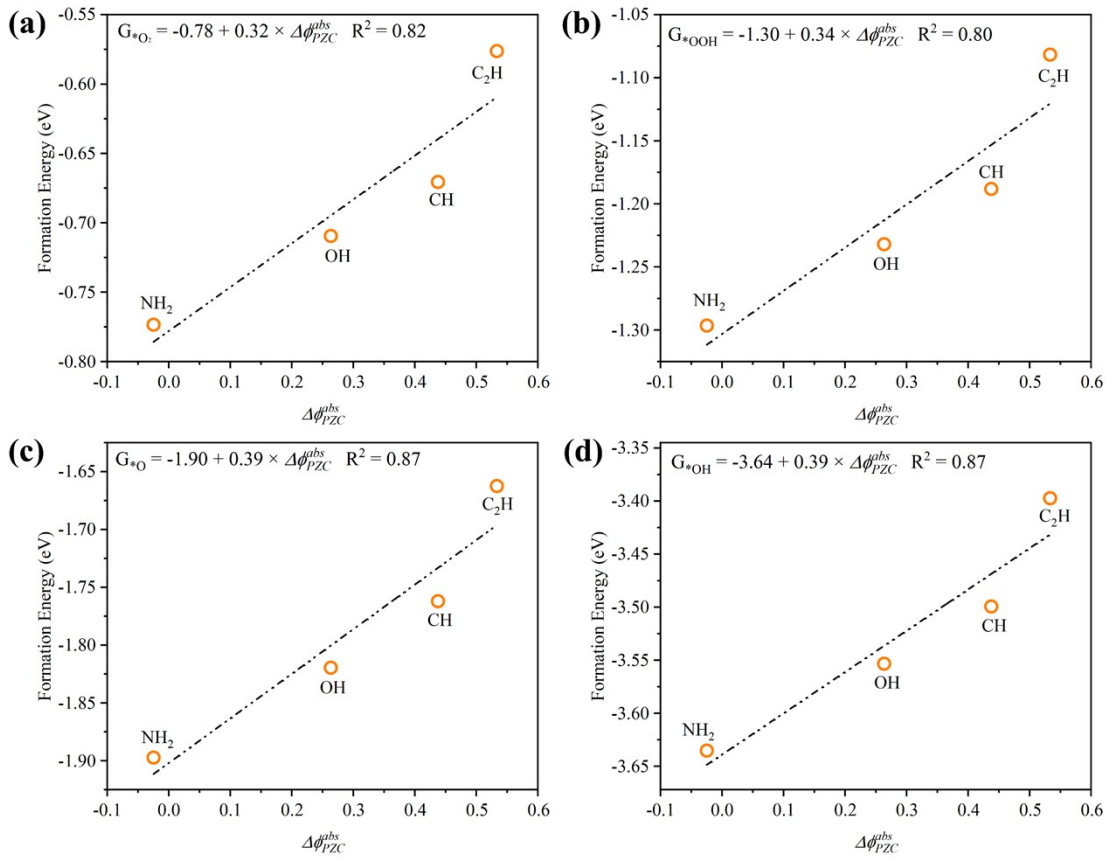

Figure S14: the surface charge density of the selected CoPc with -NH_2, -OH, -CH, and -C_2H termination groups as function of the adsorption energy of the O_2 (a), OOH (b), O (c), OH (d) intermediates for oxygen reduction reaction.

1. Wang, M., Torbensen, K., Salvatore, D., Ren, S., Joulié, D., Dumoulin, F., ... & Robert, M., CO_2 electrochemical catalytic reduction with a highly active cobalt phthalocyanine. *Nat. Commun.* **2019,** *10* (1), 3602-3610.

2. Zhang, X., Wu, Z., Zhang, X., Li, L., Li, Y., Xu, H., ... & Wang, H., Highly selective and active CO_2 reduction electrocatalysts based on cobalt phthalocyanine/carbon nanotube hybrid structures. *Nat. Commun.* **2017,** *8* (1), 14675-14683.

3. Han, N.; Wang, Y.; Ma, L.; Wen, J.; Li, J.; Zheng, H.; Nie, K.; Wang, X.; Zhao, F.; Li, Y.; Fan, J.; Zhong, J.; Wu, T.; Miller, D. J.; Lu, J.; Lee, S.-T.; Li, Y., Supported Cobalt Polyphthalocyanine for High-Performance Electrocatalytic CO_2 Reduction. *Chem* **2017,** *3* (4), 652-664.

4. Wang, M.; Chen, L.; Lau, T. C.; Robert, M., A Hybrid Co Quaterpyridine Complex/Carbon Nanotube Catalytic Material for CO_2 Reduction in Water. *Angew. Chem. Int. Ed. Engl.* **2018,** *57* (26), 7769-7773.

5. Morlanés, N.; Takanabe, K.; Rodionov, V., Simultaneous Reduction of CO_2 and Splitting of H_2O by a Single Immobilized Cobalt Phthalocyanine Electrocatalyst. *ACS Catal.* **2016,** *6* (5), 3092-3095.

6. Lin, S., Christian S. Diercks, Yue-Biao Zhang, Nikolay Kornienko, Eva M. Nichols, Yingbo Zhao, Aubrey R. Paris et al., Covalent organic frameworks comprising cobalt porphyrins for catalytic CO_2 reduction in water. *Science* **2015,** *349* (6253), 1208-1213.
7. Wu, X.; Sun, J. W.; Liu, P. F.; Zhao, J. Y.; Liu, Y.; Guo, L.; Dai, S.; Yang, H. G.; Zhao, H., Molecularly Dispersed Cobalt Phthalocyanine Mediates Selective and Durable CO_2 Reduction in a Membrane Flow Cell. *Adv. Funct. Mater.* **2021,** *32* (11), 2107301-2107310.
8. Matheu, R., Gutierrez-Puebla, E., Monge, M. Á., Diercks, C. S., Kang, J., Prévot, M. S., ... & Yaghi, O. M., Three-Dimensional Phthalocyanine Metal-Catecholates for High Electrochemical Carbon Dioxide Reduction. *J. Am. Chem. Soc.* **2019,** *141* (43), 17081-17085.
9. Xiong, L., Fu, X., Zhou, Y., Nian, P., Wang, Z., & Yue, Q., Precise Site-Hydrophobicity Modulation for Boosting High-Performance CO_2 Electroreduction. *ACS Catal.* **2023,** *13* (10), 6652-6660.
10. Ren, S., Dorian Joulié, Danielle Salvatore, Kristian Torbensen, Min Wang, Marc Robert, and Curtis P. Berlinguette, Molecular electrocatalysts can mediate fast, selective CO_2 reduction in a flow cell. *Science* **2019,** *365* (6451), 367-369.
11. Lieber C M, L. N. S., Catalytic reduction of carbon dioxide at carbon electrodes modified with cobalt phthalocyanine. *J. Am. Chem. Soc.* **1984,** *106* (17), 5033-5034.
12. Magdesieva, T. V., Yamamoto, T., Tryk, D. A., & Fujishima, A., Electrochemical reduction of CO_2 with transition metal phthalocyanine and porphyrin complexes supported on activated carbon fibers. *J. Electrochem. Chem.* **2002,** *149* (6), 89-97.
13. De Riccardis, A.; Lee, M.; Kazantsev, R. V.; Garza, A. J.; Zeng, G.; Larson, D. M.; Clark, E. L.; Lobaccaro, P.; Burroughs, P. W. W.; Bloise, E.; Ager, J. W.; Bell, A. T.; Head-Gordon, M.; Mele, G.; Toma, F. M., Heterogenized Pyridine-Substituted Cobalt(II) Phthalocyanine Yields Reduction of CO_2 by Tuning the Electron Affinity of the Co Center. *ACS Appl. Mater. Interfaces* **2020,** *12* (5), 5251-5258.
14. Jiang, Z.; Wang, Y.; Zhang, X.; Zheng, H.; Wang, X.; Liang, Y., Revealing the hidden performance of metal phthalocyanines for CO_2 reduction electrocatalysis by hybridization with carbon nanotubes. *Nano Research* **2019,** *12* (9), 2330-2334.
15. Tian, P.; Zhang, B.; Chen, J.; Zhang, J.; Huang, L.; Ye, R.; Bao, B.; Zhu, M., Curvature-induced electronic tuning of molecular catalysts for CO_2 reduction. *Catal. Sci. Technol.* **2021,** *11* (7), 2491-2496.
16. Ma, J.-J.; Zhu, H.-L.; Zheng, Y.-Q.; Shui, M., An Insight into Anchoring of Cobalt Phthalocyanines onto Carbon: Efficiency of the CO_2 Reduction Reaction. *ACS Appl. Energy Mater.* **2021,** *4* (2), 1442-1448.
17. Zhu, H.-L.; Zheng, Y.-Q.; Shui, M., Synergistic Interaction of Nitrogen-Doped Carbon Nanorod Array Anchored with Cobalt Phthalocyanine for Electrochemical Reduction of CO_2. *ACS Appl. Energy Mater.* **2020,** *3* (4), 3893-3901.
18. Li, M.; Yan, C.; Ramachandran, R.; Lan, Y.; Dai, H.; Shan, H.; Meng, X.; Cui, D.; Wang, F.; Xu, Z.-X., Non-peripheral octamethyl-substituted cobalt phthalocyanine nanorods supported on N-doped reduced graphene oxide achieve efficient electrocatalytic CO_2 reduction to CO. *Chem. Eng. J.* **2022,** *430*, 133050-133065.
19. Zhu, M.; Ye, R.; Jin, K.; Lazouski, N.; Manthiram, K., Elucidating the Reactivity and Mechanism of CO_2 Electroreduction at Highly Dispersed Cobalt Phthalocyanine. *ACS Energy Lett.* **2018,** *3* (6), 1381-1386.

20. Luangchaiyaporn, J.; Wielend, D.; Solonenko, D.; Seelajaroen, H.; Gasiorowski, J.; Monecke, M.; Salvan, G.; Zahn, D. R. T.; Sariciftci, N. S.; Thamyongkit, P., High-performance CoII-phthalocyanine-based polymer for practical heterogeneous electrochemical reduction of carbon dioxide. *Electrochimica Acta* **2021,** *367*, 137506-137518.
21. Tian, H., Kai Wang, Ziyi Shui, Muhammad Ali Raza, Hang Xiao, Meidan Que, Liangliang Zhu, and Xi Chen, Enhanced CO_2 electroreduction on Co active site of cobalt phthalocyanine by electronic effect. *Mater. Lett.* **2022,** *310* (1), 131482-131486.
22. Gong, S., Wenbo Wang, Xinxin Xiao, Jun Liu, Chundu Wu, and Xiaomeng Lv, Elucidating influence of the existence formation of anchored cobalt phthalocyanine on electrocatalytic CO_2-to-CO conversion. *Nano Energy* **2021,** *84* (1), 105904-105915.
23. Kong, X.; Liu, G.; Tian, S.; Bu, S.; Gao, Q.; Liu, B.; Lee, C. S.; Wang, P.; Zhang, W., Coupling Cobalt Phthalocyanine Molecules on 3D Nitrogen-Doped Vertical Graphene Arrays for Highly Efficient and Robust CO_2 Electroreduction. *Small* **2022,** *18* (51), 2204615-2204624.
24. Huang, M.; Chen, B.; Zhang, H.; Jin, Y.; Zhi, Q.; Yang, T.; Wang, K.; Jiang, J., Tailored Local Electronic Environment of Co-N_4 Sites in Cobalt Phthalocyanines for Enhanced CO_2 Reduction Reaction. *Small Methods* **2024,** *9* (2), 2301652-2301660.
25. Gong, S.; Han, X.; Li, W.; Zhao, G.; Zhai, Y.; Wang, W.; Xia, Q.; Wang, X.; Wu, J.; Wu, C.; Lv, X.; Zhang, X., Paired electrolysis for efficient coproduction of CO and S_8 with techno-economic analysis. *Chem. Eng. J.* **2025,** *507* (1).
26. Ding, J.; Wei, Z.; Li, F.; Zhang, J.; Zhang, Q.; Zhou, J.; Wang, W.; Liu, Y.; Zhang, Z.; Su, X.; Yang, R.; Liu, W.; Su, C.; Yang, H. B.; Huang, Y.; Zhai, Y.; Liu, B., Atomic high-spin cobalt(II) center for highly selective electrochemical CO reduction to CH_3OH. *Nat. Commun.* **2023,** *14* (1), 6550-6560.
27. Wang, Q.; Chen, J.; Pan, H.; Liu, W.; Liu, Y.; Chen, B.; Qi, D.; Wang, K.; Jiang, J., Modulating Active Center Microenvironment in Phthalocyanine-Based Covalent Organic Frameworks for Enhanced Electrocatalytic CO_2 to CH_3OH. *Adv. Mater.* **2025,** *37* (21), 2502644-2502654.
28. Cheon, S.; Li, J.; Wang, H., In Situ Generated CO Enables High-Current CO_2 Reduction to Methanol in a Molecular Catalyst Layer. *J. Am. Chem. Soc.* **2024,** *146* (23), 16348-16354.
29. Shi, G.; Zhang, W.; Kang, Y.; Zhao, J.; Lu, T.; Yang, C.; Chang, M.; Shen, Y.; Gao, X.; Wu, J.; Li, Y.-F.; Cao, K.; Zhang, L., Nanoconfinement promotes CO_2 electroreduction to methanol on a molecular catalyst. *Nat. Commun.* **2025,** *16* (1), 7359-7369.
30. Song, Y.; Musgrave, C. B.; Su, J.; Huang, L.; Guo, W.; Liu, Y.; Li, G.; Xin, Y.; Zhang, Q.; Feng, X.; Liao, C.; Liu, S.; Kwok, R. T. K.; Lam, J. W. Y.; He, M.; Choong, K. S.; Feng, Z.; Tang, B. Z.; Goddard, W. A.; Ye, R., Efficient CO_2-to-methanol electrocatalysis in acidic media via microenvironment-tuned cobalt phthalocyanine. *Nat. Nano.* **2025**, 1-9.
31. Zanotti, G.; Palmeri, F.; Raglione, V.; Khodadadi, A.; Tabaries, C.; Capitolis, J.; Prevot, M.; Piccolo, L.; Zendehdel, M.; Flammini, R.; Contini, G., Eco-Friendly Synthesis of Cobalt Phthalocyanine for High-Efficiency CO_2 Electroreduction. *Chem. Eur. J* **2025,** *1* (1), 02264.
32. Wu, Y., Zhan Jiang, Xu Lu, Yongye Liang, and Hailiang Wang, Domino electroreduction of CO_2 to methanol on a molecular catalyst. *Nature* **2019,** *575* (7784), 639-642.
33. Zhu, Q.; Rooney, C. L.; Shema, H.; Zeng, C.; Panetier, J. A.; Gross, E.; Wang, H.; Baker, L. R., The solvation environment of molecularly dispersed cobalt phthalocyanine determines methanol selectivity during electrocatalytic CO_2 reduction. *Nat. Catal.* **2024,** *7* (9), 987-999.
34. Li, J., Quansong Zhu, Alvin Chang, Seonjeong Cheon, Yuanzuo Gao, Bo Shang, Huan Li et al.,

Molecular-scale CO spillover on a dual-site electrocatalyst enhances methanol production from CO_2 reduction. *Nat. Nano.* **2025,** *18* (1), 1-8.

35. Li, J., Shang, B., Gao, Y., Cheon, S., Rooney, C. L., & Wang, Mechanism-guided realization of selective carbon monoxide electroreduction to methanol. *Nat. Synthesis* **2023,** *2* (12), 1194-1201.